Design and implementation of sun tracking system for parabolic dish solar collector

Gonzalo G. Fernandez

I. Introduction

Concentrating solar power (CES) is a promising renewable energy source. By concentrating the sun's rays on a small area, CES systems can reach very high temperatures. This characteristic presents them as a suitable option not only for electricity generation, but also for industrial applications where a high temperature heat source is required.

Parabolic solar concentrators (PSCs) are CES systems consisting of a reflecting surface in the shape of a paraboloid of revolution, a support structure, a receiver and a solar tracking system, with the receiver located at the focal point of the paraboloid of revolution. The tracking system keeps its axis parallel to the sun's rays. In this way, the radiation passing through the circular surface determined by the contour of the disk is concentrated on the receiver. The receiver converts the concentrated solar radiation into heat, reaching temperatures up to 1500°C, and that heat is transferred to a heat transfer fluid (HTF). The FTC delivers the energy to the desired application, and can range from air, oils, to phase changing fluids such as salts or metal alloys.

The province of Mendoza has great potential for PSC development. Global solar radiation reaches a monthly average of 7.5 kWh/(m2 day) in December, has a minimum of 2.5 kWh/(m2 day) in July and represents 1.8 MWh /m2 in a year.

Juan Manuel Leiva's doctoral work analyzes the use of a PSC with the objective of producing high temperatures. The PSC was built from a satellite antenna of the grating type and its dimensions are approximately 3m in diameter and 0.8m deep, and it is available at the Institute of Space Training and Computer Aided Engineering Development (CEDIAC) at the Faculty of Engineering of the Universidad Nacional de Cuyo.

The geometry used by this PSC requires the solar tracking system to be more accurate than the one used in conventional systems. For this reason, students from the Mechatronics Engineering program at the Faculty of Engineering of the Universidad Nacional de Cuyo have collaborated in the development of a solar tracking system with high precision.

II. Description of the requirements for the solar tracking system

The parabolic axis of the dish must be kept parallel to the sun's rays in order to reflect them into the receiver aperture. Therefore, a two-axis sun tracking system capable of orienting the parabolic dish to compensate for the movement of the sun in the sky is required.

Various designs of support structures and sun-tracking systems exist. The PSC considered in this work has an altitude-azimuth configuration, as seen in Fig. 2.

Fig. 1. Parabolic solar concentrator (PSC)

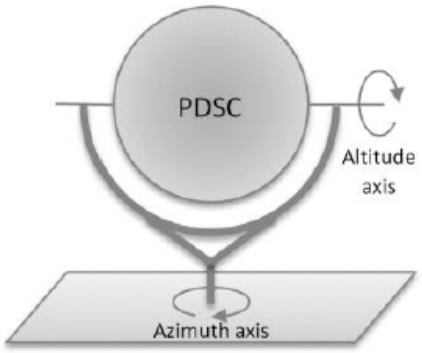

Fig. 2. PSC support structure configuration

With the chosen design, simulations were carried out in previous works taking into account the solar radiation of Mendoza in order to determine the necessary precision in each of the axes for different values of desired absorption performance. To perform such calculations, the so-called astronomical equations were used, which allow, from the coordinates of the device location and the current date and time, to obtain the values of the desired azimuthal and elevation positions. As previously mentioned, in the case of the PSC it is imperative that the axis of the PSC coincides with the axis of the sun's rays.

Fig. 3 and Fig. 4 show the result of the simulation for a misalignment of 1°degree of the axis. In Fig. 3 the incident rays that are reflected and captured by the receiver are shown

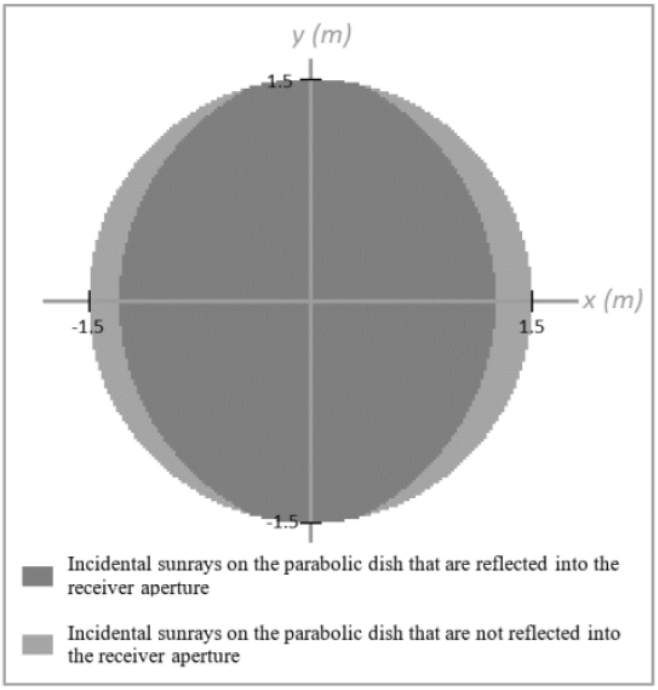

Fig. 3. Simulation results for 1° of misalignment: reflected rays

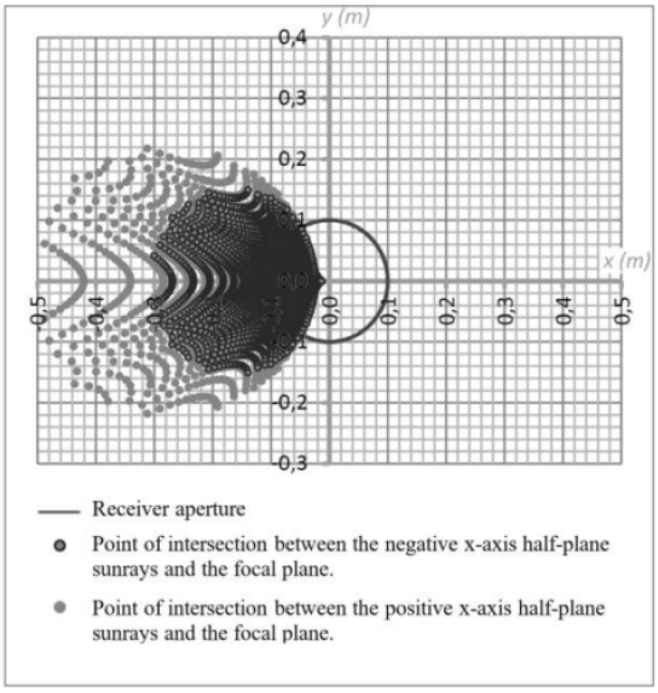

Fig. 4. Simulation results for 1° misalignment: intersection of rays with focal plane

in dark and those that are not are shown in light. In Fig. 4, for the same misalignment, the diameter of the receiver is shown in solid line, in dark tone the points of intersection of the rays with the focal plane that are absorbed and in light tone those that are not.

Several tests were performed and the alignment efficiency, i.e. the percentage of incident solar rays on the PSC that are exploited, was calculated in each case. Some values obtained are shown in Table I. This method only considers the efficiency loss due to misalignment and assumes that the reflecting surface is perfectly parabolic. The PSC intercept factor is affected by the misalignment and the optical quality of the surface. It was found that to achieve an alignment efficiency of 100.00% the misalignment between the PSC axis and the solar rays must be less than 0.246 degree. Furthermore, the alignment efficiency and thus the overall efficiency of the PSC are highly sensitive to the alignment accuracy. A misalignment of 1.00° reduces the alignment efficiency to 83.93%. Also in the analysis it is concluded that the alignment accuracy requirements are more relaxed when the parabolic dish is shallower.

Disalignment	**Number of incident rays in the PSC**	**Number of reflected rays at the receiver**	**Efficiency of alignment**
0.246°	17593	17593	100.00%
0.250°	17593	17591	99.99%
0.300°	17593	17512	99.54%
0.500°	17593	16774	95.34%
0.750°	17593	15730	89.41%
1.000°	17593	14765	83.93%

TABLE I
CALCULATED ALIGNMENT EFFICIENCIES

III. INITIAL PROJECT STATUS

A conceptual schematic of the proposed electronic design implemented in the 2018 work of Delgado and Rivier [1] can be seen in Fig. 5.

The main element is an Arduino Mega development board with an Atmega2560 microcontroller. The board communicates with the PC via USB connection, with UART serial communication, and makes use of two modules: a DS3231 real time clock (RTC) module, and an SD memory module. In addition, the microcontroller sends control signals to two Pololu DRV8825 drivers that drive each stepper motor of the mechanical system. The power supply to the Arduino board is through the 5V USB, and the power supply to the stepper motors is through an external 12V power supply.

A more detailed description of the above components follows:

The **driver DRV8825**, which can be seen in Fig. 6 is an integrated that allows the control of bipolar stepper motors. It operates with motor voltages from 8.2V to 45V, and without any additional dissipation it can supply 1.5A per coil. In the implementation of the work, heatsink was placed on each of the modules, so they can supply currents up to 2.2A per coil without risking damage from overheating. Motor movement is achieved by pulsing the STEP input and setting the module's DIR input to a logical voltage value. In addition, the driver provides the possibility of using different step resolutions (from 1 to 1/32) and also the possibility of adjusting the maximum current value allowed by means of a potentiometer. The module has an integrated voltage regulator, so a power supply for the logic is not necessary, as the power supply of the motors is sufficient.

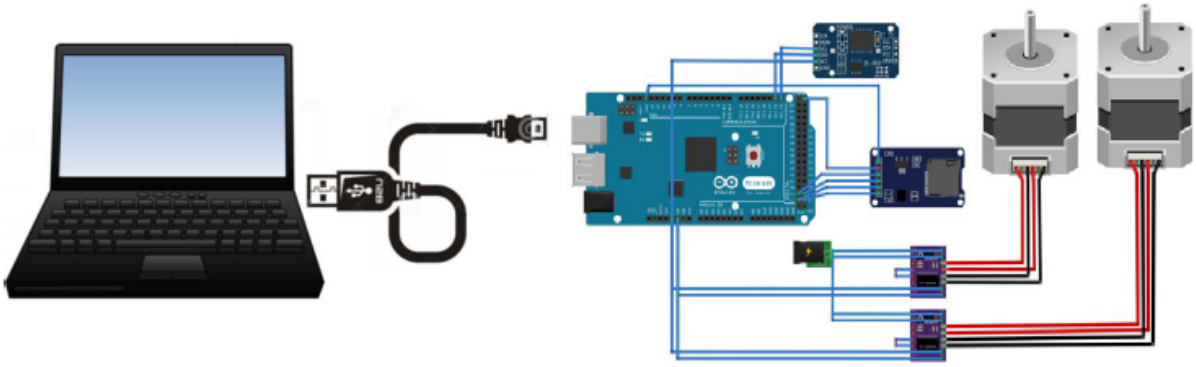

Fig. 5. Conceptual schematic of the initial electronic design

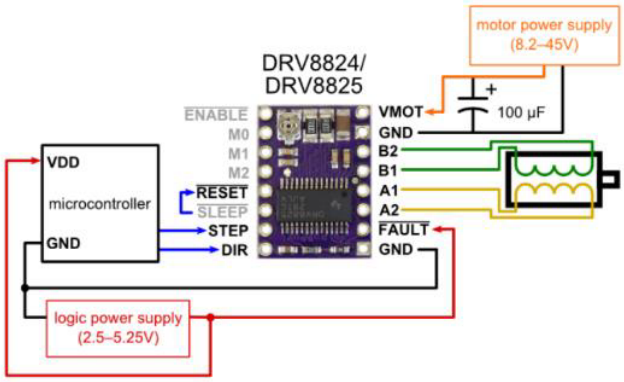

Fig. 6. DRV8825 driver basic connection scheme

The **DS3231 RTC module**, which can be seen in Fig. 7, contains a MAXIM model DS3231 real-time clock from MAXIM, an Atmel AT24C32 EEPROM and an integrated temperature sensor. It also includes the pull-up resistors necessary for communication via I2C protocol and an internal voltage regulator that allows the module to be powered with a logic voltage of 5V, which is more usual than 3.3V. Access to the date and time is via I2C interface, using the device's write and read addresses and accessing the RTC's own registers that store the values. The time can be set in 12 or 24 o'clock format and has a leap year compensation. It also has two configurable alarms that are not used in the project. Unlike other similar models, the DS3231 uses its temperature sensor to make a compensation that gives it great accuracy (about 2 minutes per year). The module's battery has a discharge time of about 2 years, so it does not present any inconvenience for its application in the project.

The **SD Card module**, which can be seen in Fig. 8, allows reading and writing of memory cards of type SDSC (standard capacity) or SDHC (high capacity) formatted in FAT16 or FAT32 file systems. The communication of the module with the microcontroller is via the SPI interface which allows a high transfer rate. The module can be powered with 3.3V, but it also has an integrated voltage regulator and can be powered with 5V.

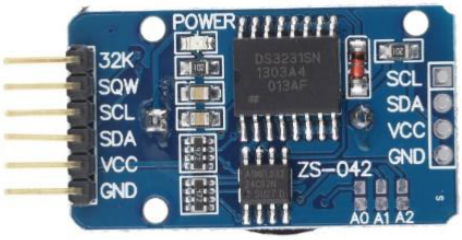

Fig. 7. Module with real time clock RTC DS3231

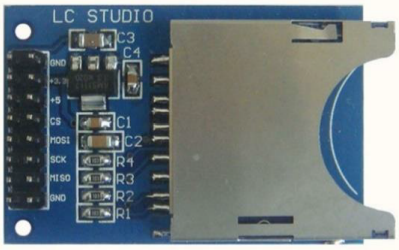

Fig. 8. Module for SD memory

A. *First mechanical prototype*

In Fig. 9 can be seen the first prototype designed for the project, developed by Delgado and Rivier [1] and then used for the evaluation of the final algorithm by Palau [2].

It is a simple design, consisting of 3 pieces manufactured with 3D printing in PLA plastic: A base with four legs on which the motor corresponding to the azimuth axis is mounted, a "U" shaped piece that is placed under pressure on the azimuth motor axis and where the motor corresponding to the elevation axis is mounted, and then a last piece that is placed under pressure on the elevation motor axis and on which the camera used by the closed-loop algorithm is mounted at its end.

The bipolar stepper motors are model EM-462 reused from a disused EPSON printer, so their specifications are not available. They can be seen in Fig. 10.

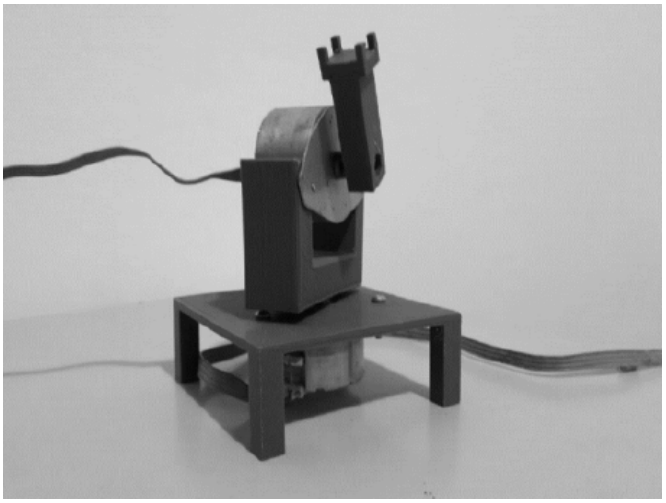

Fig. 9. First mechanical prototype

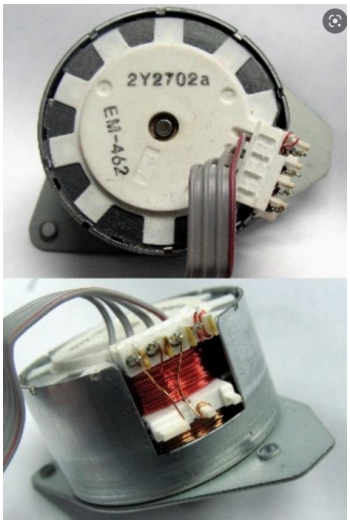

Fig. 10. Epson EM-462 bipolar stepper motor

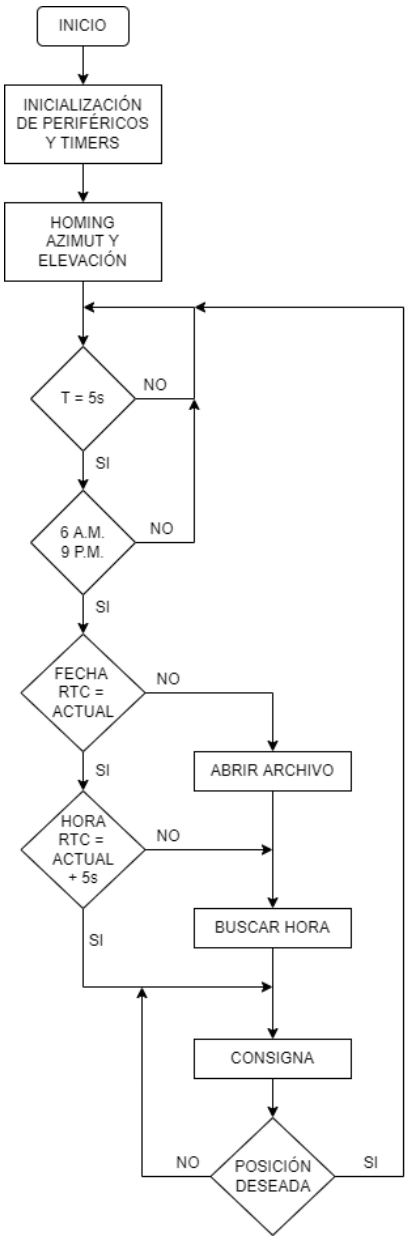

Fig. 11. Flowchart of open-loop control algorithm

B. Open-loop control algorithm

A description of the open-loop control algorithm developed by Delgado and Rivier [1] for the sun-tracking system is given below. In Fig. 11 the flowchart exposing the algorithm operation can be observed.

In the first instance, the peripherals and timers used throughout the application are initialized. The addresses of the microcontroller registers that handle the limit switches (inputs) and the direction and step pulses of the motor drivers (outputs) are specified.

A first timer of the microcontroller is configured to generate interrupts every one second. This interruption increments a counter that updates the time and date of the system every five interruptions, i.e., every five seconds the information is updated. The time and date are obtained from the RTC.

A second timer is configured to generate interrupts every 10ms. In its interrupt, by using the functions for reading and writing FAT file systems (used in the SD card), different flags are set to synchronize, with the corresponding times, the transmission and reception of data from the card.

A third and fourth timer are configured to generate the square wave received by the azimuth and elevation motor drivers. The pulses are counted in the corresponding interrupt routines which, according to the general state of the program, are enabled or disabled.

The microcontroller is responsible for sensing the limit switches via pins configured with external interrupts. The interface with the RTC is through I2C communication with a SCL frequency of 100kHz. The UART communication with the PC is done with a baud rate of 57600 bits per second, and the data reception is configured by interrupt in order not to occupy the CPU with a polling process. The SPI peripheral is initialized to be able to interact with the SD card module.

Before starting the main loop of the application, the homing of both motors is performed, with an average speed deter-

mined, in counterclockwise motion, until the end of stroke is detected. Then, for greater homing precision, a clockwise movement is performed, with a speed determined as slow, until the limit switches are no longer detected.

The application is based on a finite state machine defined by the following states: *new date*, *new time* and *new setpoint*. The state is updated within the interrupt routine of the first timer described (the one associated with the time and date update).

If the time is not within 6:00 A.M. and 9:00 P.M. the two motors are left in their homing positions, otherwise the following situations are checked: If the date differs from the previous one, the current date is updated with that of the RTC and the status *new date* is activated; if the time differs by more than five seconds from the previous one, the current time is updated based on the one provided by the RTC and the status *new time* is activated; finally if neither the date nor the time differs from the previous one, the time is updated and the status *new setpoint* is activated.

After homing, when entering the main loop, different tasks are executed depending on the active state. If the state machine is in *new date*, the file name is generated, the file is read from the SD and the state is reset. If the active state is *new time*, the line number to be read from the file is calculated, the file is scrolled until the desired line is found and then parsed to obtain the azimuth and elevation setpoint. If the active state is *new setpoint* the next line to the current position in the open file is read and the position setpoints are parsed and updated.

Finally, the time and date of the RTC module can be updated in order to initialize the clock value, which is set to zero by default.

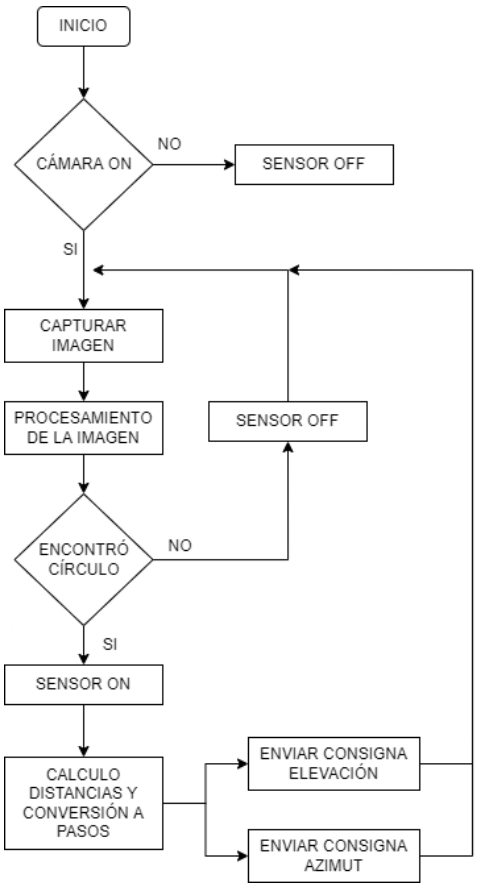

Fig. 12. Closed-loop control algorithm flow chart

C. Computer vision-based closed-loop control algorithm

The following is a description of the computer vision-based sensor developed by Palau [2] for closed-loop control of the tracking system. In Fig. 12 the flowchart exposing the operation of the sensor and its interaction with the open-loop control system can be observed.

When the sensor is connected, it is first checked if the camera is working. If it is not, a signal is sent to the open loop control informing that the sensor is off. This signal, and any other signals sent by the sensor, are communicated via UART. If, on the other hand, the camera is working properly, an image is captured, processed and checked for a circle in the image. If it is negative, the sensor off signal is sent and a new image is captured. If a circle was detected, the sensor on signal is sent, the setpoints are calculated and we proceed to verify which setpoint was sent in the last iteration. If the elevation setpoint was sent then the azimuth setpoint is sent and vice versa. Once the setpoint has been sent, another image is captured and the process is repeated.

For more information on the processing performed on the image captured by the camera go to the work of Palau [2].

IV. Objectives and work plan

The initial objectives set forth were: to collaborate in the final details of the construction of a functional prototype; and to design the electrical board and printed circuit board (or PCB) of the sun tracking system, with power, communication and control subsystems.

Therefore, the activities to be performed consisted of the following:

- Study the sensor and control algorithm already implemented.
- Transition the PC implementation of the project software to a microprocessor (Raspberry Pi).
- Design and build a printed circuit board incorporating all the electronics of the tracking system.
- Design and build an electrical board with the corresponding safety elements.
- Mount and calibrate the sensor on the structure of the sun-tracking system.

V. Software and hardware integration

VI. Prototype design and fabrication

The first prototype designed by Palau [2] for the project was presented in the section **??**. It has the great advantage of being simple both in design and construction due to its simple geometry, a fundamental characteristic at that stage of the project where the first tests of the tracking system had to be carried out quickly.

However, at the current stage of the project, where a much more advanced control algorithm is available and it is necessary to obtain definitive results to define the viability of

the tracking system, the great importance of having a device that mechanically does not present problems and on which all the necessary tests and experiments can be carried out dynamically and comfortably is recognized.

One of the first conflicts reported by Palau [2] when carrying out his experiments was the deformation of the base piece when the prototype was subjected to the Sun. Looking at Fig. 9 it can be seen that this part is thin and it is logical that the heating produced by the solar energy deforms the part quickly.

When familiarizing with the previous state of the project it was also detected that in general the size of the prototype was very small (to give an idea of the size the base was approximately 65mm x 65mm) for the functions it had to fulfill, which can be summarized as holding and moving a webcam with its USB cable. In addition, press-fitting the parts onto the motor shafts is not the best fastening mechanism, the parts slip, glue had to be applied to fix them, and therefore it was not reliable to ensure the solidity between the part and the shaft.

Another important point to highlight is the direct relation of the motor on the movement in azimuth or elevation. On the prototype control has the advantage that if the motors do not lose steps during a given trajectory, the final position is reliable and data can be obtained as it happens in the work of Palau [2]. However, if one reflects on the main objective of a prototype which is to obtain a preliminary version of a device under development, in this case to scale, where one tries to recreate as reliably as possible its operation, it is exposed that the 1:1 ratio of the prototype is not a faithful representation of the real system, which has a chain drive with 488:1 gear ratio in the azimuth axis and 588:1 in the elevation axis.

Once the shortcomings of the first prototype were detected in order to continue with more advanced evaluations of the tracking system, a second prototype was designed from scratch using the same stepper motors as the first one.

The first step in the design of the second prototype was to propose a transmission ratio. In addition to correcting the previously mentioned shortcoming of fidelity in the real system, the gear ratio has the additional advantage of allowing the motor to operate at a higher angular velocity for the same angular velocity of shaft movement (either azimuth or elevation) compared to a direct ratio. This translates into the motor being able to operate over a wider range of speeds and, therefore, generate a smoother motion on the final shaft.

The proposed transmission system was through double helical gears, also called herringbone gears. The choice is motivated by the benefit of compensating misalignments present in the system that, given the tools with which the prototype will be manufactured, which are not of great precision, will exist in one way or another. The system proposed for the azimuth axis transmission can be seen in Fig. 13.

Following the basic formula for gear design,

$$D_p = Z \cdot m \tag{1}$$

Where D_p is the primitive diameter of the gear, Z the number of teeth and m the module, the gear system is designed with module 1.5 and gear ratio 1:3. A 20-tooth drive gear, resulting in a 30mm pitch diameter, and a 60-tooth driven gear, resulting in a 90mm pitch diameter, are proposed. Both the azimuth and elevation systems have the same system.

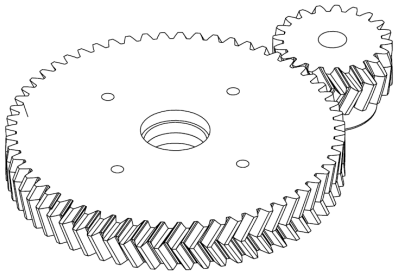

Fig. 13. Double helical transmission system

Fig. 15 shows in an exploded view how the drive gear is mounted on the stepper motor shaft.

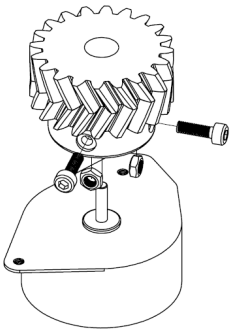

Fig. 14. Exploded view of motor and motor gear

It consists of two M3 nuts that are inserted into slots in the gear body, on which two M3 bolts are then threaded so that through the nuts they press the gear body against the stepper motor shaft. This already solves one of the shortcomings of the first prototype mentioned previously.

Incorporating a transmission system on both axes offers the advantages already mentioned but, on the other hand, it also adds complexity to the system. One of the aspects to consider is the design of the shaft on which the driven gear and the associated body rotate. If there is a lot of friction between the shaft and the base on which it rotates, the stress on the motor increases, since it must not only overcome the inertia of the body but also the associated friction. To reduce this friction, bearings are incorporated in the design. The bearings selected for this task are of the deep groove ball type, model 608-2Z, as they are suitable in their dimensions and also very common both in the local market and in articles such as skates.

In Fig. 15 can be seen an exploded view of the driven body of the azimuth system, in other words the first link of the mechanism. It can be seen how the mentioned bearings are mounted, and how the different parts are assembled into a single rigid body by means of 4 M4 bolts and nuts.

In Fig. 16 can be seen an exploded view of the complete azimuth system, i.e., the mounting of the motor, motor gear, driven gear and the associated body on the designed base can be seen. For this purpose, the motor with its gear are fitted to

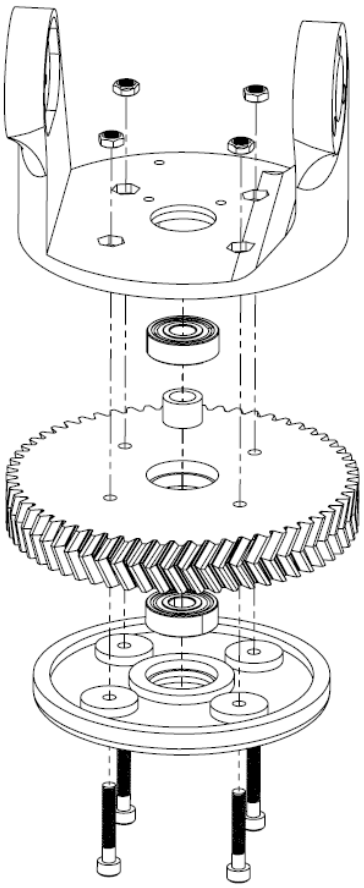

Fig. 15. Exploded view of first link

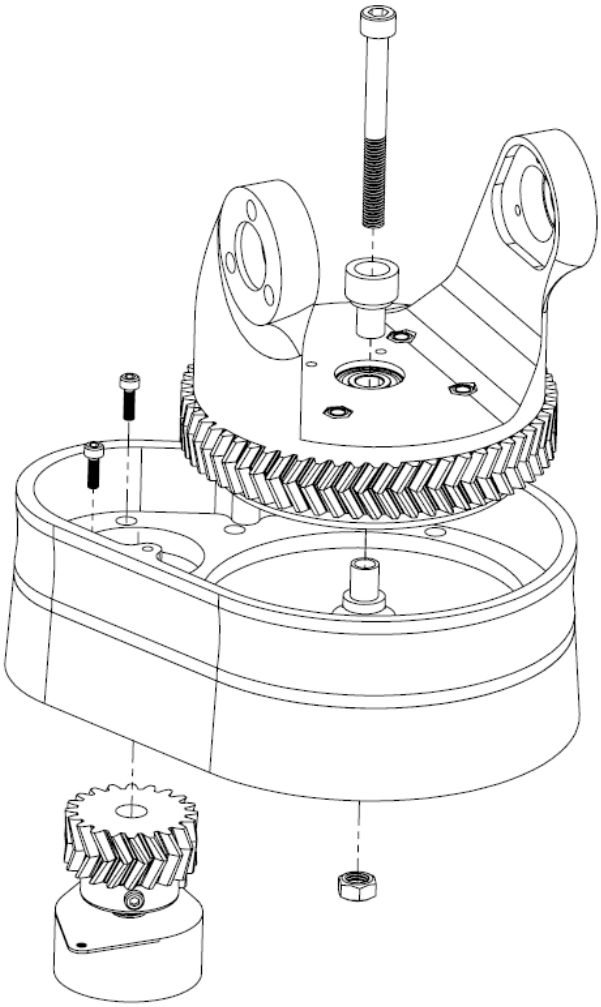

Fig. 16. Exploded view of the system for azimuth movement

the base by means of two M3 screws, and then the driven body is mounted on the base by the shaft object, which consists of a 60mm long M6 screw with its corresponding nut.

Once the azimuth system was completed, its operation could be individually evaluated. There it was concluded that the fabrication provides adequate precision for the transmission system to function properly and, in addition, that the motor used has sufficient torque to rotate the structure.

In Fig. 17 an exploded view can be seen that allows understanding the way in which the part that allows incorporating the motor associated to the elevation shaft to the system is assembled. This part is rigidly attached to the first link of the mechanism by means of 3 M3 screws. Then the motor with the corresponding gear, identical to that of the azimuth system and assembled as shown in Fig. 17, is fitted to the part by means of two M3 screws.

As in the azimuth shaft, deep groove ball bearings 608-2Z are also used in the elevation shaft to reduce friction in its rotation. In Fig. 18 can be seen an exploded view that exposes the placement of these bearings, which remain rigid on the first link by covering them with a piece that is adjusted by three M3 bolts with the corresponding nuts.

In Fig. 19 it can be seen in an exploded view the way in which the elevation shaft is assembled. Basically it consists of a double helical driven gear of the same characteristics and dimensions of the one used in the azimuth system only that, considering that the articular range does not need to be greater than 180°degree (during the day the sun always stays above the horizon), 210°degree of the gear is used. An M6 threaded rod is used as a shaft, on which the gear is fitted by means of M3 bolts and nuts. On the shaft is also placed the body in charge of holding the camera in place. This body is fitted to the shaft by means of 6 M3 screws with their corresponding nuts. The ends of the shaft are fitted over the bearings of the first link by means of spacers and 3D printed caps.

In Fig. 20 a view of the complete assembly can be seen, i.e., the azimuth axis and the elevation axis mounted. All that remains is to place a part on the body placed on the elevation axis that will allow mounting the specific camera to be used in the prototype.

VII. Sensor calibration mechanism

As mentioned in section I, and being the objective pursued in the developments of Delgado and Rivier [1] and Palau [2], for the construction of the solar collector to be feasible the alignment error of the parabola axis must be kept below 0.25°. In the two works mentioned above, the prototype is

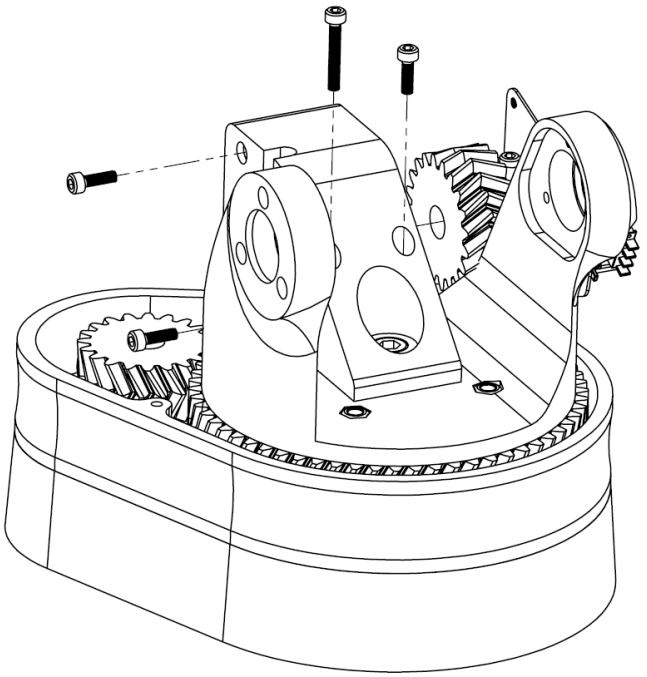

Fig. 17. Exploded view of elevation shaft motor

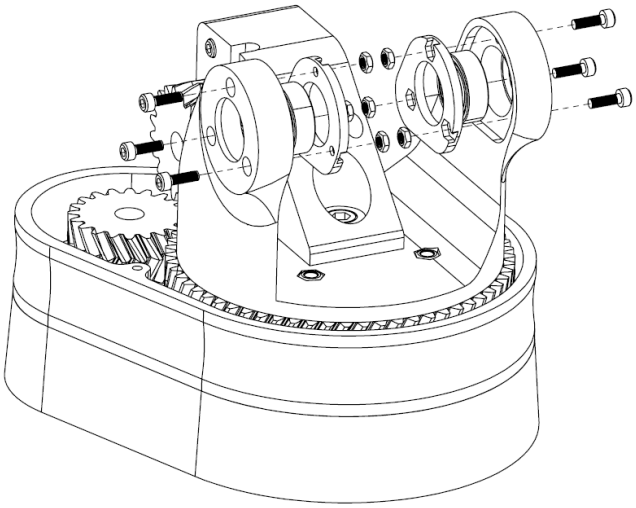

Fig. 18. Exploded view of elevation shaft bearings

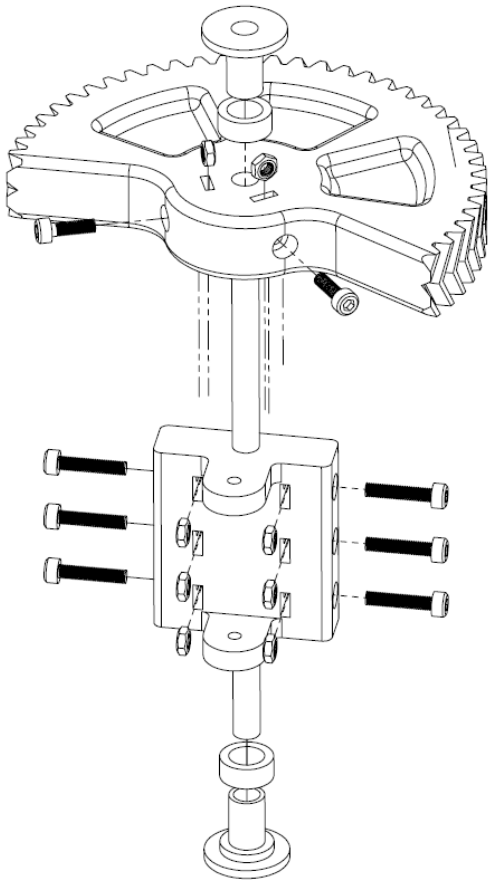

Fig. 19. Exploded view of elevation axis

kept aligned with the sun with an acceptable margin of error, however, when placing the system with the computer vision based sensor on the real system, the problem of aligning the parabola axis with the "axis" of the camera being used in the sensor arises with a new different margin of error.

This issue was discussed with the director of the work and the following process was conceptually proposed: On a vertical wall at a given distance from the structure with the sensor, arrange marks in a trigonometrically determined location with the axis of the parabola by placing the structure horizontally; with the parabola horizontal, direct the sensor camera towards the wall in such a way that the mark enters the captured image; vary the orientation of the system with the camera relative to the parabola so that the mark is positioned in the center of the image.

This is why it was necessary to develop a mechanism that allows the camera orientation to be varied for system calibration. The accuracy of this mechanism is important, since the calibration error is added or complemented to the parabola axis alignment error. When discussed with the director of the work, it was concluded that the calibration mechanism should tolerate errors of at most 10 times the misalignment error of the parabola, i.e., it should be able to orient the camera with an accuracy of at least 0.025°.

VIII. Results and conclusions

In the initial work plan, as expected results it was proposed to finish the activity in the project with a functional prototype and, in addition, to have a board that integrates the electrical and electronic systems operating in conjunction with the mechanical system.

A photograph of the second prototype manufactured can be seen in Fig. 23.

A second prototype was obtained which, despite not being a final design, solved all the shortcomings pointed out about the first one without increasing the economic cost of its manufacture. This is so because, with the exception of the PLA plastic used in the 3D printing, the rest of the components were

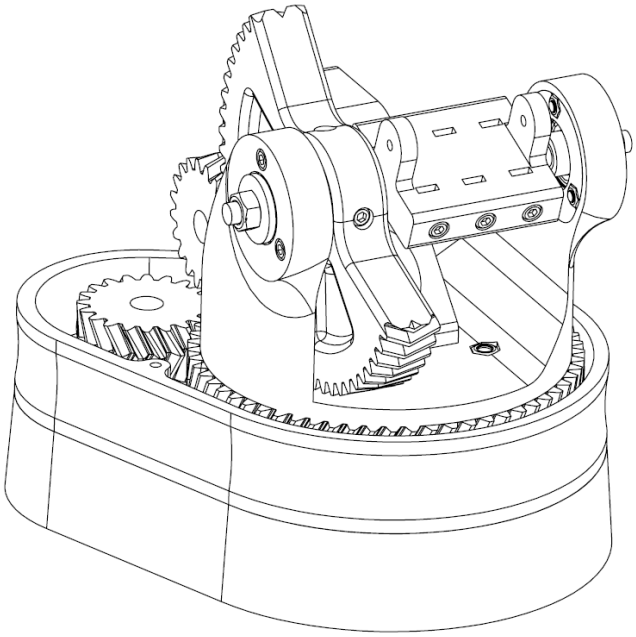

Fig. 20. Complete assembly view of second prototype

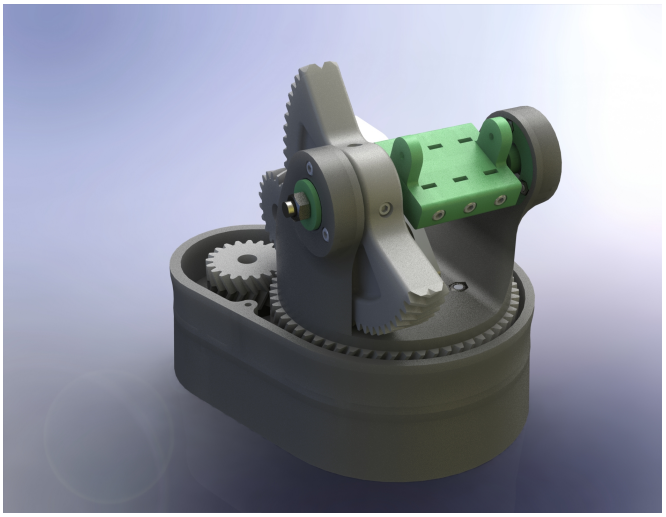

Fig. 21. Rendering of the complete assembly of the second prototype

reused: the 608-2Z bearings are very common in items such as skates, and the nuts, the screws and the threaded rod are reused elements from disused electrical and electronic devices.

When 3D printing the various parts of the second large prototype, it is recommended to use an extruder nozzle of at least 0.8mm diameter. This will greatly reduce the printing time, which with a 0.4mm diameter nozzle can take more than 24 hours. The gears are not included in this group, since they have a high level of detail in their teeth that is lost with a wide extruder nozzle, but it does include parts such as the base, the body of the first link, the adapter of the lifting motor on the first link, etc.

Finally, for proper operation it is recommended to incorporate some lubricant to the drive systems, such as solid petroleum jelly. This reduces noise, friction between the gears

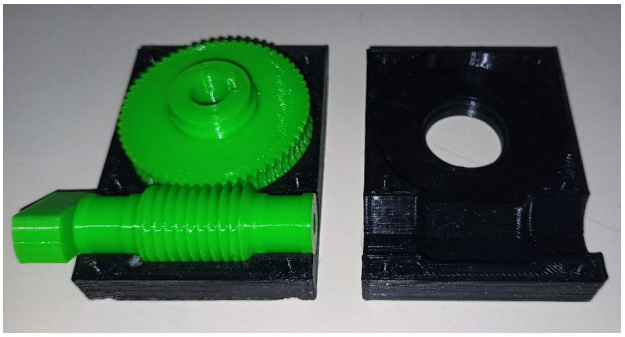

Fig. 22. Initial auger test with additive manufacturing

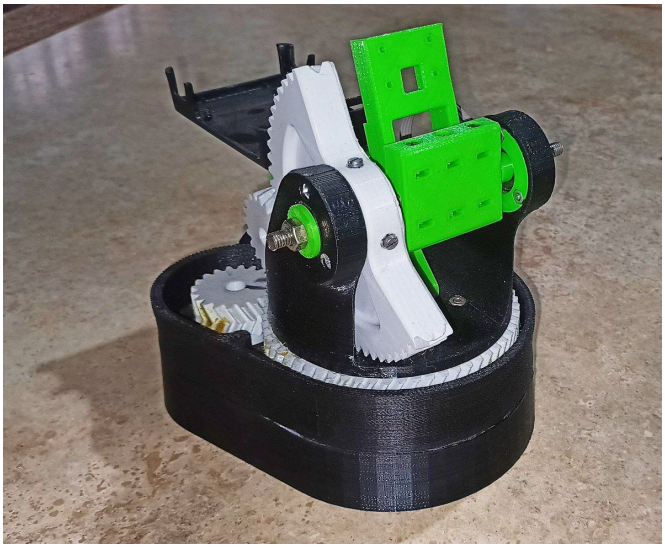

Fig. 23. Photo of the second prototype manufactured

and, therefore, decreases the stress on the motors and results in a smoother movement.

IX. Future work

In the design of the second prototype drive systems, two aspects can be analyzed for consideration in the design of a third prototype in the future. The first aspect is backlash, i.e., the backlash or loss of motion of the drive system caused by the gap between the gears. Such a gap, given the manufacturing method, is difficult for a gear system to eliminate and leads to an end position error that is difficult to correct. Replacing the gear drive system to a belt drive system can be contemplated. However, a belt drive system leads to the complexity of adding, for example, a belt tensioning mechanism. The second aspect, which in turn works against the choice of a belt drive system in the prototype, is the large difference of the gear ratio value with that of the real system. It is very difficult to achieve such high reduction values with the proposed systems, the use of a planetary reduction system could be considered where high reduction values are achieved but its design and manufacturing is considerably more complex.

In addition, the sensor calibration mechanism must be further developed, manufactured and experimental tests carried

out once the construction of the structure with the parabola is completed.

References

[1] Lautaro Delgado and Santiago Rivier. “Mecanismo de Seguimiento Solar de un Colector Solar Parabólico”. In: *Investigación en Ingeniería* (2018).

[2] Franco Palau. “Diseño y Construcción de un SIstema de Seguimiento del Sol para Colector Solar de Disco Parabólico”. In: *Investigación en Ingeniería* (2019).